Article

Flow Boiling Heat Transfer of R134a in a Horizontal Smooth Tube: Experimental Results, Flow Patterns, and Assessment of Correlations

Ernest Gyan Bediako *, Petra Dančová * and Tomáš Vít

Department of Power Engineering Equipment, Faculty of Mechanical Engineering, Technical University of Liberec, 461 17 Liberec, Czech Republic
* Correspondence: ernest.gyan.bediako@tul.cz (E.G.B.); petra.dancova@tul.cz (P.D.);
Tel.: +420-776-037-976 (E.G.B.)

Abstract: This study presents an extensive evaluation of heat transfer characteristics, flow patterns, and pressure drop for saturation pressures ranging from 460–660 kPa in a horizontal smooth tube of 5 mm internal diameter using R134a as the working fluid. The effect of saturation pressures for mass fluxes of 150–300 kg/m^{2}s and heat fluxes of 8.26–23.3 kW/m^2 which are typical of refrigeration and air conditioning applications are also investigated. Flow patterns observed during the study are predicted with a well-known flow pattern map of Wojtan et al. The experimental results are compared with seven (7) correlations developed based on different theories to find which correlation best predicts the experimental data. The results show that, at low mass flux, increasing saturation pressure results in an increased heat transfer coefficient. This effect is more pronounced in the low vapor quality region and the dominant mechanism is nucleate boiling. At high mass flux, increasing saturation pressure leads to an insignificant increase in the heat transfer coefficient. At this high mass flux but low heat flux, the heat transfer coefficient increases with vapor quality, indicating convective boiling dominance. However, for high heat flux, the heat transfer coefficient is linear over vapor quality, indicating nucleate boiling dominance. Pressure drop is observed to decrease with increasing saturation pressure. Increasing saturation pressure increases the vapor quality at which the flow pattern transitions from intermittent flow to annular flow. The flow patterns predicted are a mixture of slug and stratified wavy and purely stratified wavy for low mass fluxes. For increased mass fluxes, the flow patterns predicted are slug, intermittent, annular, and dryout. Cooper's model was the best predictor of the experimental data and the trend of heat transfer coefficient.

Keywords: flow boiling; heat transfer coefficient; heat flux; mass flux; saturation pressure; pressure drop; flow pattern; two-phase flow

1. Introduction

Over the past few years, many researchers in the field of air conditioners and refrigeration applications have become more interested in flow boiling heat transfer using small diameter tubes, especially investigating the accurate determination and prediction of heat transfer coefficient, pressure drop, flow patterns, and understanding of the dominant mechanism controlling the heat transfer. This is because understanding flow boiling heat transfer plays a significant role in the optimal design of evaporators for heat exchangers in air conditioners and refrigeration systems [1–4].

For flow boiling heat transfer, two mechanisms, namely nucleate boiling and convective boiling, are assumed to control the heat transfer which then relates to the heat transfer coefficient and flow patterns significantly. Nucleate boiling is said to dominate the heat transfer when bubbles generated at the walls of the tube are responsible for controlling the heat transfer. Convective boiling on the other side is assumed to dominate the heat transfer

when conduction and convection processes occurring at the thin liquid layer near the wall and liquid–vapor interface, respectively, control the heat transfer [5,6].

These heat transfer mechanisms are highly affected and controlled by flow parameters such as working fluid, the geometry of the tube, saturation conditions (temperature and pressure), mass flux, heat flux, and vapor quality [7].

For the effect of flow parameters on heat transfer coefficient, when saturation conditions and heat flux affect the heat transfer coefficient significantly, nucleate boiling is considered to dominate and control the heat transfer. When mass flux and vapor quality significantly affect the heat transfer coefficient, convective boiling is considered to dominate and control the heat transfer [8,9]. Both mechanisms can co-occur over a wide range of vapor quality where the heat transfer coefficient is affected by mass flux, heat flux, and saturation conditions along certain regions of vapor quality [7,10].

Despite extensive studies on flow boiling heat transfer, the general characteristics and dominant mechanism responsible for controlling the heat transfer remain enigmatic with many contradicting results for seemingly similar experimental conditions reported in the literature [11,12]. According to [13], although several studies have been performed to understand the effect of flow parameters on heat transfer characteristics there is still a lack of consensus on how these flow parameters and their interrelations affect heat transfer behavior during flow boiling with many contradicting results and complex trends of heat transfer coefficient along a range of vapor quality.

Saturation conditions such as saturation pressure and temperature have a significant influence on the boiling properties of heat transfer, however, according to [14], less attention has been given to their direct influence on heat transfer characteristics during flow boiling in small-diameter tubes. Much of the concern is about how saturation conditions influence the heat transfer mechanism and the trend evolution of the heat transfer coefficient with varying vapor quality, heat flux, and mass fluxes.

For example, some studies report an increasing effect of saturation conditions on the heat transfer coefficient [15–18]. Greco and Vanoli [15] investigated the flow boiling heat transfer characteristics of R134a in a smooth horizontal tube of 6 mm internal diameter. They considered saturation pressures of 300–1200 kPa, the mass flux of 360 kg/(m^{2}s), and heat fluxes of 11–21 kW/m^2. Their study reported that the heat transfer coefficient increased with increasing saturation pressure. With the trend of heat transfer coefficient versus vapor quality, they reported that the heat transfer coefficient decreased to a minimum in the low-quality region and increased in high vapor quality region, signifying the dominance of nucleate boiling in the low-quality region and convective boiling in the high vapor quality annular region. They further concluded that, at high heat fluxes and saturation pressures, nucleate boiling dominated the heat transfer. However, at low heat flux and saturation pressure, convective boiling was the dominant mechanism controlling heat transfer.

Celen and Dalkilic [16] also evaluated the effect of operating parameters such as saturation pressure, mass flux, heat flux, and vapor quality on the heat transfer coefficient of R134a working fluid for a horizontal tube of 8.62 mm internal diameter. They evaluated the effect of saturation pressures of 490–600 kPa, the mass flux of 290–381 kg/(m^{2}s), and a heat flux of 10–15 kW/m^2. They concluded that increasing saturation pressure resulted in an increasing heat transfer coefficient. With the trend of heat transfer coefficient with vapor quality, their study indicated an increasing trend of heat transfer coefficient over the entire vapor quality range.

Another study by Eckels and Pate [17] investigated the heat transfer characteristics of R134a in an 8 mm internal diameter tube. The flow boiling study was performed for a saturation pressure range of 248–390 kPa for a mass flux of 125–400 kg/(m^{2}s) and a heat flux of 12 kW/m^2. Their study reported that the heat transfer coefficient increased significantly with increasing saturation pressure. Xu et al. [18] experimentally evaluated the effect of mass fluxes of 185–935 kg/(m^{2}s), heat fluxes of 18–35.5 kW/m^2, and saturation pressures of 578–820 kPa on flow boiling heat transfer characteristics of R134a in a 4.065 mm internal diameter tube. Their study concluded that the heat transfer coefficient increased

significantly with increasing saturation pressure. They reported an almost linear trend of the heat transfer coefficient over the entire range of vapor qualities until dryout was reached.

Some experimental studies also report a negligible effect of saturation conditions on the heat transfer coefficient [19–21]. For example, Grauso et al. [20] presented an experimental investigation in a 6 mm internal diameter smooth stainless steel tube for a saturation pressure of 264–450 kPa, the mass flux of 146–520 kg/(m²s), and heat fluxes of 5–20.4 kW/m². The working fluid was R134a. They investigated the effect of these conditions on the heat transfer coefficient and reported that increasing saturation pressure did not have any significant effect on the heat transfer coefficient. However, it was observed that, with the trend of the heat transfer coefficient with vapor quality, the heat transfer coefficient decreased slightly to a minimum at around vapor quality of 0.5 before increasing over the entire vapor quality range until dryout is reached. They reported that this observation indicated the dominance of nucleate boiling in the low vapor quality region and convective boiling in the high vapor quality region. Guo et al. [19] also investigated the flow boiling heat transfer characteristics of R134a at saturation pressures of 1379–3608.3 kPa in a 10 mm internal diameter tube. They considered heat fluxes of 6–24 kW/m² and mass fluxes of 100–300 kg/m²s. They reported that increasing saturation pressure did not produce any significant change in the heat transfer coefficient. However, with the trend of heat transfer coefficient versus vapor quality, it was observed that the heat transfer coefficient increased with increasing vapor quality until dryout. Saitoh et al. [21] investigated the boiling heat transfer of R134a in a horizontal small diameter tube of 3 mm. Their study measured the heat transfer coefficient and pressure drop for saturation pressures of 350–488 kPa, the mass flux of 150–450 kg/m²s, and the heat flux of 5–29 kW/m². Their results concluded that saturation pressure had a negligible effect on the heat transfer coefficient for the conditions investigated. They reported an increasing trend of the heat transfer coefficient with vapor quality over the entire vapor quality range until dryout is reached.

It is interesting to observe that some experimental studies even reported a decreasing effect of saturation pressure on the heat transfer coefficient. For example, Balachander and Raja [22] investigated the flow boiling heat transfer characteristics of R134a for saturation pressures of 164–293 kPa in a 7.49 mm internal diameter. Their study considered mass fluxes of 57–102 kg/(m²s) and a heat flux of 7.5 and 8.3 kW/m². They reported that increasing saturation pressure decreased the heat transfer coefficient. Their results indicated a decreasing trend of the heat transfer coefficient with vapor quality. They also reported that nucleate boiling was the dominant mechanism controlling heat transfer.

Results from the literature review above indicate that increasing saturation pressure has a varying effect on the heat transfer coefficient and different studies report different effects. Some studies reported an increasing effect of saturation pressure on the heat transfer coefficient, some reported a negligible effect of saturation pressure on the heat transfer coefficient and others even reported a decreasing effect. It can be concluded that there is no consensus on the effect of saturation conditions on heat transfer characteristics. The same can be said about the dominant mechanism controlling the heat transfer and trend evolution of the heat transfer coefficient as a function of vapor quality for increasing saturation pressure which has been observed to vary without any agreed trend. Some studies report an increasing trend of the heat transfer coefficient with vapor quality, some report a decreasing trend, some report a linear trend, and others report a combination of these trends.

There are many correlations in literature for predicting flow boiling heat transfer in small diameter tubes; a fact that confirms that the actual mechanism responsible for controlling the heat transfer is still not clear and agreed upon [23,24]. These many correlations are designed based on different theories with many adjusting parameters [25]. Refs. [24,26] evaluated different correlations and concluded that various correlations poorly predicted the experimental data investigated during flow boiling for different interrelations of saturation conditions, mass fluxes, heat fluxes, and vapor qualities.

This study, therefore, presents an extensive evaluation of the heat transfer coefficient, flow patterns, and pressure drop for three saturation pressures in a horizontal smooth tube of 5 mm internal diameter, using R134a as the working fluid. The study investigated the effect of saturation pressure for a mass flux of 150–300 kg/(m²s) and heat flux of 8.26–23.3 kW/m² which are typical of refrigeration and air conditioning applications. The flow patterns observed during the study were predicted with a well-known flow pattern map. The experimental results were compared with seven (7) correlations developed based on different theories to find which correlation best predicts the experimental data. This included pool boiling type, superposition type, enhancement approach, asymptotic approach, and largest mechanism type. Table 1 summarizes the experimental investigations reviewed above for flow boiling in a horizontal smooth tube and the effect of saturation pressure on the heat transfer coefficient.

Table 1. Summary of experimental studies on flow boiling for R134a in horizontal smooth tubes.

Author(s)	Fluid Type	Experimental Set Up	P_sat (kPa)	G (kg/m²s)	q″ (kW/m²)	Effect of Saturation Pressure on HTC
Greco and Vanoli [15]	R134a	6 mm ID, horizontal smooth tube, 6 m length	300–1200	360	11–21	Increases
Celen and Dalkiliç [16]	R134a	8.62 mm ID horizontal smooth tube	488.75–609.17	290–381	10–15	Increases
Eckels and Pate [17]	R134a	8.0 mm ID, horizontal smooth tube	350–490	125–400	9.1	Increases
Xu et al. [18]	R134a	4.065 mm ID, Horizontal smooth tube	578–820	185–935	18–35.5	Increases
Grauso et al. [20]	R134a	6 mm ID, horizontal smooth tube	264.11–445.59	146–520	5–20.4	Negligible
Guo et al. [19]	R134a	10 mm ID, Horizontal smooth tube	1379–3608.3	100–300	6–24	Negligible
Saitoh et al. [21]	R134a	3.1 mm ID, horizontal smooth tube	350–488	150–450	5–39	Negligible
Balachander and Raja [22]	R134a	7.49 mm ID, horizontal smooth tube	164–293	57–102	2–18	Decreases

2. Experimental Setup and Procedure

2.1. Experimental Setup

As described in [8,27], the experimental setup was a closed loop system with a main tank for storing refrigerant, a magnetic coupled gear pump for distributing the refrigerant, a preconditioner for controlling the vapor quality of the fluid at the inlet of the test section, a visualization glass for visualizing the flow, an adiabatic and diabatic test section, and a condenser for cooling the refrigerant during the experiment from the test section. The schematic representation of the test facility is shown in Figure 1. R134a was the working fluid for this study. Saturation condition in the store tank controls the pressure in the test section. The inlet temperature of the refrigerant is controlled by a shell and tube heat exchanger with glycol flowing in the shell side. A Coriolis mass flow meter installed before the heated test section was used to measure the flow rate of the refrigerant before it enters the test section. The test section shown in Figure 2 is a 5 mm internal diameter, 8 mm outer diameter, and 2035 mm-long stainless steel is supplied with heat by the Joule effect with a rectified sine wave. The test section was heavily insulated against heat losses to the external environment. With the test section, ten (10) thermocouples were fitted externally on the lower section and seven (7) on the upper section. At specific location, 1117 mm and 1917 mm from the inlet thermocouples, internal thermal thermocouples were fitted on the

top, bottom, and side walls of the tube. Variables such as temperatures, absolute pressures, differential pressure, and mass flow rate were obtained at a frequency of 10 Hz. The data were acquired with the LABVIEW National Instrument data acquisition system.
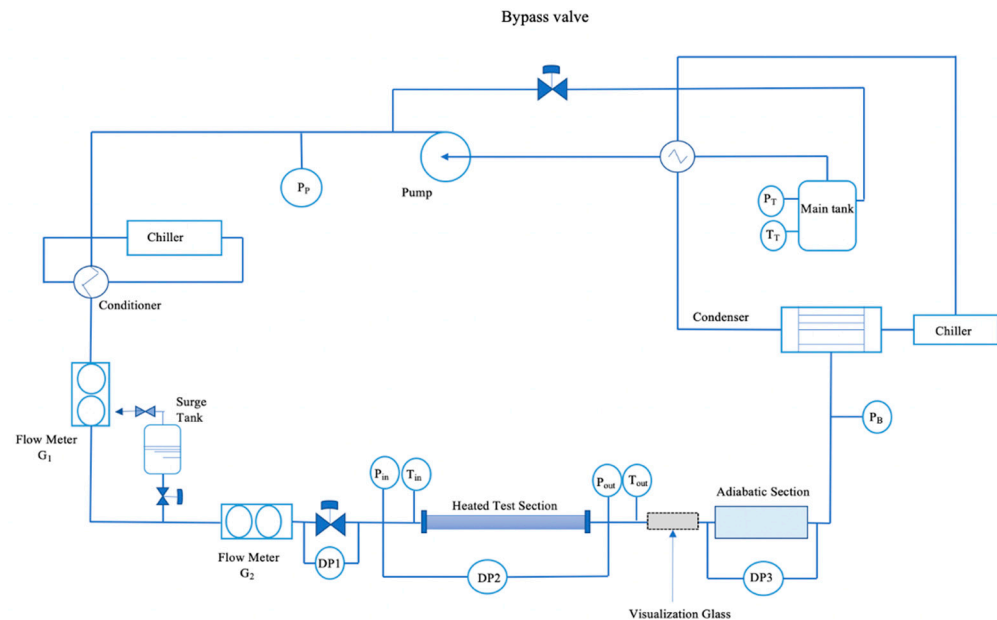

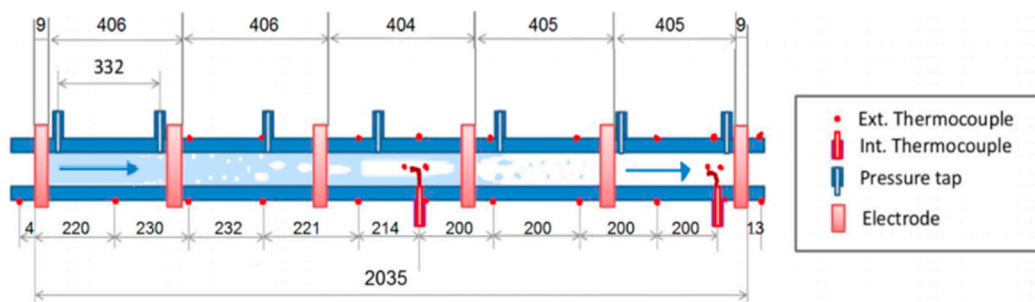**Figure 1.** Schematic representation of the test facility.

Figure 2. Schematic representation of the test section.

The operation procedure for this experiment:
- The facility was first heated up with the highest proposed power in the heated test section.
- The pressure at the outlet of the heated test section was maintained constant.
- The experimental data for each point were collected only after steady-state condition was reached. Steady-state condition for the experiment was said to be reached when the time variation in the mass flux, pressure, and inlet temperature was less than 6% for about 200 s.
- After reaching the highest proposed power, the supplied heat was decreased systematically. By decreasing the supplied heat, each measurement point was obtained.
- Each experimental data was recorded for 100 s and this corresponded to 1000 points. The process of first heating up to the planned power before reducing the power for each point helps to avoid an abrupt rise in the wall temperature when onset of nucleate boiling occurs or changes occur in the flow pattern. This also helps in the repeatability of the experiment.

With two-phase pressure drop measurement, a differential pressure was used.

The image of the schematic representation of the test facility and test section is shown in Figures 1 and 2.

2.2. Accuracy of Measurement

Tables 2–4 summarize the measurement accuracy, uncertainties of the parameters, and experimental conditions for this experimental study, respectively. The thermophysical properties of R134a refrigerant calculated with REFPROP software (9.1) [28] are found in Table 5. The electrical heat supplied to the pipe was first calibrated against thermal heat flowing to the fluid under stationary conditions but at varied temperatures and flow rates for single-phase liquid flow.

Table 2. Measurement accuracy.

Variable	Symbol	Accuracy	Information
Mass flux	G	0.2% of the reading	Given by supplier
Pressure drop	ΔP	0.075% full scale (fs = 50 kPa)	Given by supplier
Absolute pressure	P	0.04% full scale (fs = 25 bar)	Given by supplier
Temperature	T	0.1 K	Inhouse calibration
Heat flux	q''	3% of the reading	Inhouse calibration

Table 3. Uncertainties of the main operational parameters.

Parameter	Symbol	Error
Mass flux	G	$\pm 10 \ \text{kg/m}^2\text{s}$
Inlet pressure	P_i	$\pm 10 \ \text{kPa}$
Inlet temperature	T_i	$\pm 0.2 \ ^\circ\text{C}$
Heat flux (all 5 zones)	q''	$\pm < 40 \ \text{W}$

Table 4. Working condition for this experimental study.

Working Condition	Unit	Range
Saturation Pressure	kPa	460–660
Mass flux	$\text{kg/(m}^2\text{s)}$	150–300
Heat flux	kW/m^2	8.26–23.3
Vapor quality	-	0.1–1.0

Table 5. Thermophysical properties for R134a at saturation pressure of 460 kPa, 560 kPa, and 660 kPa.

Properties	Saturation Pressure (460 kPa)	Saturation Pressure (560 kPa)	Saturation Pressure (660 kPa)
Saturation temperature ($^\circ$C)	13.50	19.33	24.73
Liquid density (kg/m^3)	1250.00	1227.8	1207.7
Vapor density (kg/m^3)	22.397	27.2	32.1
Liquid enthalpy (kJ/kg)	217.92	226.5	234.16
Vapor enthalpy (kJ/kg)	406.06	409.4	412.2
Liquid viscosity (Pa.s)	2.258×10^{-4}	2.09×10^{-4}	1.96×10^{-4}
Vapor viscosity (Pa.s)	1.1219×10^{-5}	1.1462×10^{-5}	1.1682×10^{-5}
Liquid conductivity (mW/m K)	86.247	83.572	81.251
Vapor conductivity (mW/m K)	12.690	13.271	13.798
Surface tension (mN/m)	9.6121	8.7804	8.0669

2.3. Data Reduction

By performing heat balance along the heated test section, vapor quality is determined by:

$$x(z) = \frac{\int_{z_0}^{z} q'' \, \pi D_i dz - G \, A \, cp_l T_{sub}}{G \, A \, h_{lv}} \tag{1}$$

where $x(z)$ is the vapor quality at location z (m) along the heated test section. $G \ (\text{kg/(m}^2\text{s)})$ is the mass flux, h_{lv} (J/kg K) is the enthalpy of vaporization, $A \ (\text{m}^2)$ is the cross-sectional

area of the tube, cp_l (J/(kg K)) is the heat capacity of the liquid phase fluid, and T_{sub} (K) is the inlet subcooling.

The local heat transfer coefficient, measured at position 1917 mm from the inlet of the test section for each measurement was determined by Newton's law of cooling. This is given as:

$$h = \frac{q''}{T_{w,i} - T_f} \tag{2}$$

where h $\left(\text{W}/\text{m}^2\text{K}\right)$ is the heat transfer coefficient, q'' $\left(\text{W}/\text{m}^2\right)$ is the inner wall heat flux, T_f (K) is the fluid bulk temperature, and $T_{w,i}$ (K) is the inner wall temperature.

The total heat flux supplied to the flowing fluid is given by the total heat divided by the total heated length inner surface area given by the relation:

$$q'' = \frac{P}{\pi D_i \Delta z} \tag{3}$$

Here, q'' $\left(\frac{\text{W}}{\text{m}^2}\right)$ is the heat flux to the flowing fluid, P (W) is the total amount of electrical power supplied, D_i (m) is the inner diameter of the heated section, and Δz (m) is the heated section's length where the electrical power is supplied. A voltage potential was provided to the heated section by 6 electrodes distributed at every 0.4 m on the heated test section. The power was supplied by a means of low voltage and high current sine wave that have been rectified. The signal duty was used to regulate the quantity of power. The total electrical heat supplied is determined by:

$$P = I_{RMS} U_{RMS} \tag{4}$$

where I_{RMS} is the root mean square values of the electrical current and U_{RMS} is the root mean square values of the voltage signals. The heated sections are properly insulated and the volumetric heat created in the pipe wall is forced to flow to the flowing fluid.

2.4. Validation

In order to verify the reliability of the experimental facility, single phase liquid and vapor heat transfer coefficient results from this facility were compared with the Dittus–Boelter correlation given as:

$$Nu = 0.023 Re^{0.8} Pr^{0.4} \tag{5}$$

where Nu is the Nusselt number, Re is the Reynolds number, and Pr is the Prandtl number. The resulting comparison is shown in Figure 3. It can be seen that the single phase heat transfer coefficient results were within ±30% of that predicted by the Dittus–Boelter correlation.
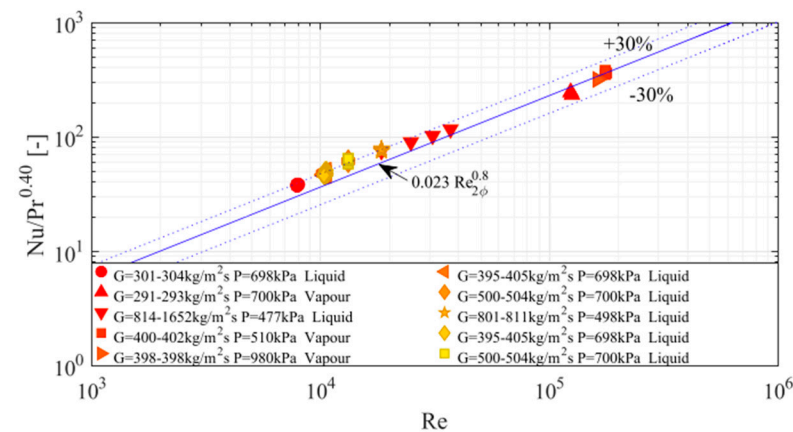

Figure 3. Single-phase heat transfer experimental results versus predictions by Dittus–Boelter.

With two-phase flow boiling validation, a case of mass flux (G) of 200 kg/m^{2}s, heat flux (q$''$) of 4.6 kW/m^2, and saturation pressure of 460 kPa from the experimental facility was compared with a similar condition in literature. The resulting comparison is shown in Figure 4. From the comparison, it can be deduced that the facility produced satisfactory results, and therefore, the results from this facility can be trusted.
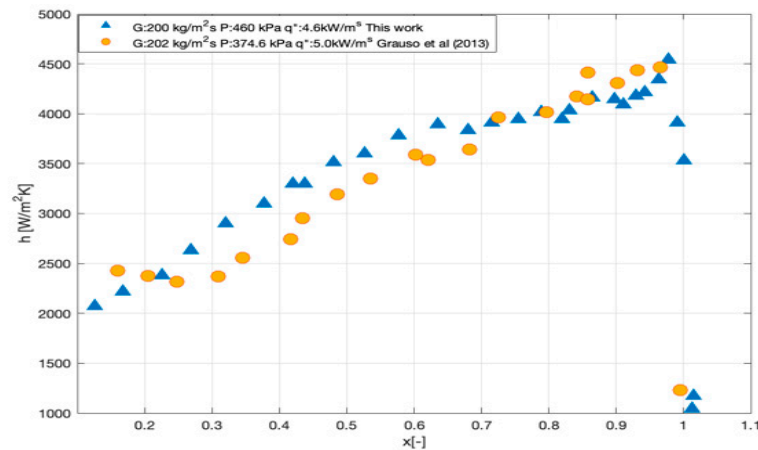

Figure 4. Comparison of two-phase heat transfer experimental results from this facility with similar cases from literature [20].

3. Results and Discussion

This study sought to investigate the characteristics of the heat transfer coefficient at three saturation pressures. Flow patterns were predicted with a well-known flow pattern map from Wojtan et al. [29] for the experimental conditions studied. The experimental results were compared with some popular flow boiling correlations developed based on different theories.

3.1. Flow Boiling Heat Transfer Coefficient

Figure 5 shows the effect of saturation pressure on the heat transfer coefficient for a low mass flux of 150 kg/m^{2}s and a heat flux of 8.26 kW/m^2. From the results, it can be seen that the heat transfer coefficient increases with increasing saturation pressure. The effect of saturation pressure on the heat transfer coefficient is more pronounced in a low vapor quality region of around 0.4 and below. However, for the characteristics of the heat transfer coefficient with increasing vapor quality, the heat transfer coefficient decreases slightly in the low-vapor quality region up to around x = 0.3 before it increases steadily and almost collapses into a single plot in the high vapor quality region until dryout occurs. Before dryout incipience, the heat transfer coefficient rises sharply to a maximum before deteriorating in the dryout region. Because the heat transfer coefficient highly depends on saturation pressure in the low vapor quality region, nucleate boiling heat transfer thus dominates the heat transfer in this region. As vapor quality increases, the dominances of nucleate boiling are suppressed, leading to the reduced effect of saturation pressure. This characteristic of the heat transfer coefficient is observed because increasing saturation pressure decreases surface tension. This then leads to an increase in the number of active sites for nucleation to occur. The frequency of bubble generation thus increases with many bubbles generated in smaller sizes on the heating walls of the tube. Additionally, increasing saturation pressure has an increasing effect on vapor density and a decreasing effect on liquid density which does not favor convective heat transfer. However, as vapor quality increases, these effects are suppressed, liquid film thickness reduces, and nucleate boiling dominance is suppressed.
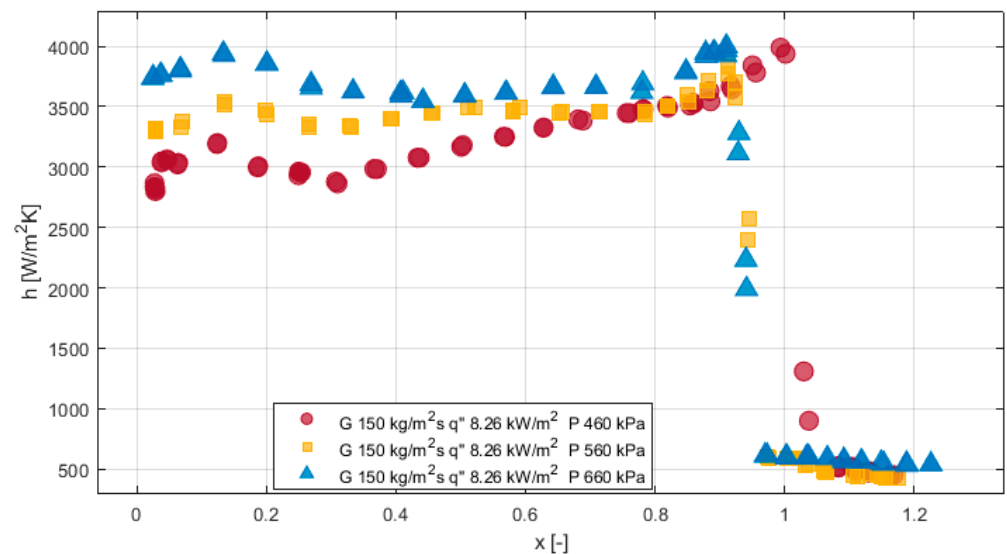
Figure 5. Effect of saturation pressure on heat transfer coefficient for mass flux 150 kg/m^{2}s and heat flux of 8.26 kW/m^2.

Figure 6 shows the effect of saturation pressure on the heat transfer coefficient for a low mass flux of 150 kg/(m^{2}s) and an increased heat flux of 23.3 kW/m^2. With an increased heat flux, it can be seen that the heat transfer coefficient increases with increasing saturation pressure over a wide range of vapor quality until dryout is reached. The trend of the heat transfer coefficient is fairly constant with increasing vapor quality. At an increased heat flux, the heat transfer coefficient is affected by saturation pressure even at high vapor qualities with minimal suppression until dryout incipience is reached. Both saturation pressure and heat flux are good promoters of nucleate boiling due to their ability to enhance bubble nucleation and bubble distribution over the walls of the tube. The dependence of the heat transfer coefficient on saturation pressure and heat flux even over a wide range of vapor quality indicates that the dominant mechanism for heat transfer, in this case, is nucleate boiling. At a vapor quality of around 0.8, dryout begins to occur with a monotonic drop in the heat transfer coefficient without a sudden rise as in the case of Figure 5.
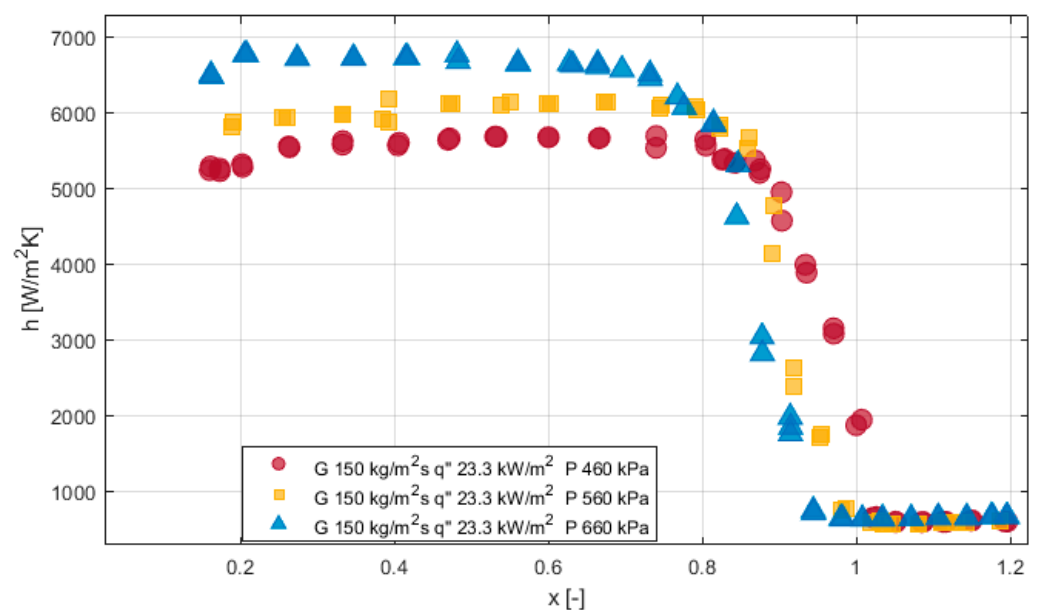

Figure 6. Effect of saturation pressure on heat transfer coefficient for mass flux of 150 kg/m^{2}s and heat flux of 23.3 kW/m^2.

Figure 7 shows the effect of saturation pressure on the heat transfer coefficient for an increased mass flux of 300 kg/m^{2}s and a low heat flux condition of 8.26 kW/m^2. For this condition, it can be seen that the heat transfer coefficient is not significantly affected by the increasing saturation pressure except for low vapor quality (x < 0.1) where there is a slight effect. However, beyond this region (x > 0.1), the heat transfer coefficient increases with vapor quality until dryout is reached. In this case, the heat transfer is dominated by convective boiling except for low vapor quality (x < 0.1) where nucleate boiling dominates the heat transfer because of the independence of the heat transfer coefficient on vapor quality. For convective boiling, an increase in mass flux increases the flow velocity and by increasing the vapor quality, the vapor phase of the two-phase flow plays a significant role in accelerating the liquid flow close to the wall of the tube and a reduced effect of the liquid phase on the heat transfer coefficient. So, in as much as increasing saturation pressure increases the vapor density and decreases the liquid density which are promoters of nucleate boiling, an increased mass flux with an increasing vapor quality is sufficient to accelerate the flow velocity, decrease the liquid film thickness near the tube wall, and thus promote convective flow boiling over nucleation. According to [23], since this convective boiling mechanism is similar to the mechanism responsible for controlling the heat transfer during single-phase flow, the same mechanism can be assumed to be controlling heat transfer during convective boiling. Contrary to many assumptions, the mechanism responsible for controlling heat transfer in a single phase is equivalent to the mechanism responsible for controlling heat transfer during convective boiling and the dominant thermal resistance is concentrated in the conductive sublayer layer.

Figure 8 shows the effect of saturation pressure on the heat transfer coefficient for a mass flux of 300 kg/m^{2}s and increased heat flux condition of 23.3 kW/m^2. It can be observed that for this condition, there is no significant effect of saturation pressure on the heat transfer coefficient except for saturation pressure of 660 kPa which shows a slight increase in the heat transfer coefficient compared to the rest. However, the trend of the heat transfer coefficient with respect to increasing vapor quality is fairly constant until dryout is reached. This indicates the dominance of nucleate boiling in controlling the heat transfer for this condition studied where bubble generation near the walls of the tube promotes the effect of nucleation.
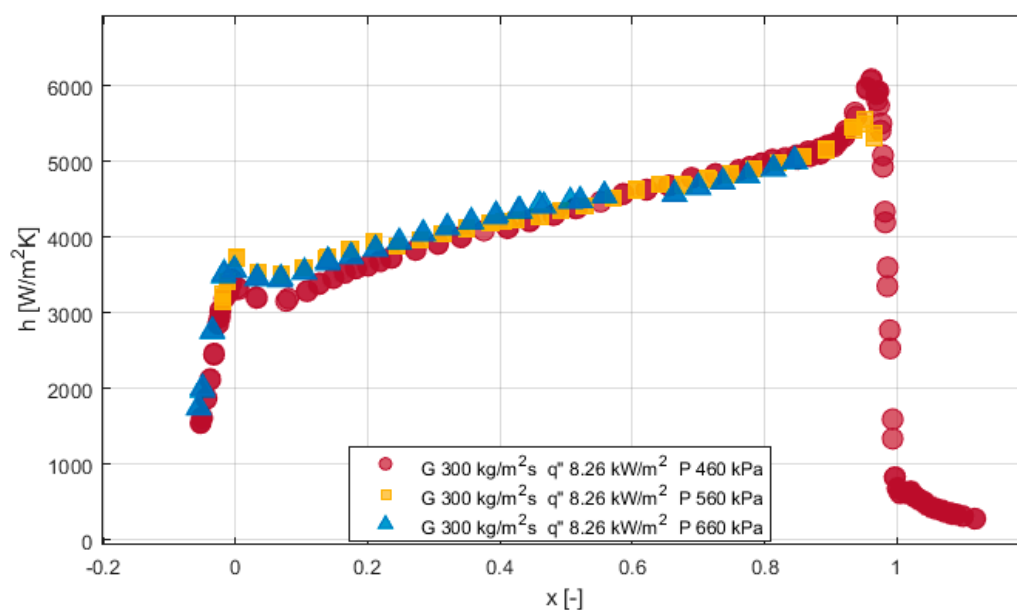

Figure 7. Effect of saturation pressure on heat transfer coefficient for mass flux of 300 kg/m^{2}s and heat flux of 8.26 kW/m^2.
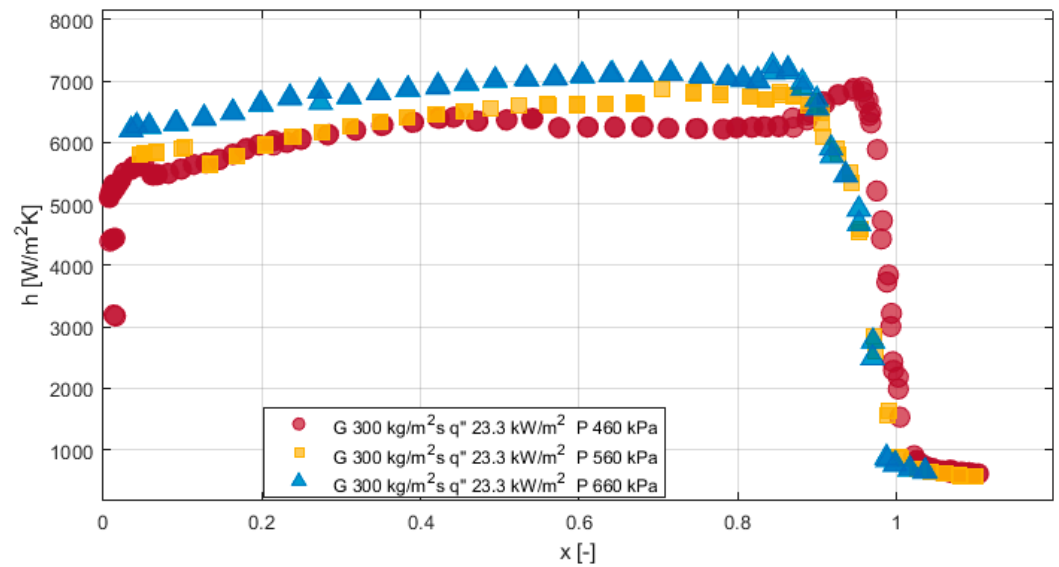
Figure 8. Effect of saturation pressure on heat transfer coefficient for mass flux of 300 kg/m^2s and heat flux of 23.3 kW/m^2.

3.2. Flow Patterns

Flow patterns for each experimental condition investigated were predicted with a well-known predictive flow pattern map from Wojtan et al. [29] shown in Figure 9a–l.
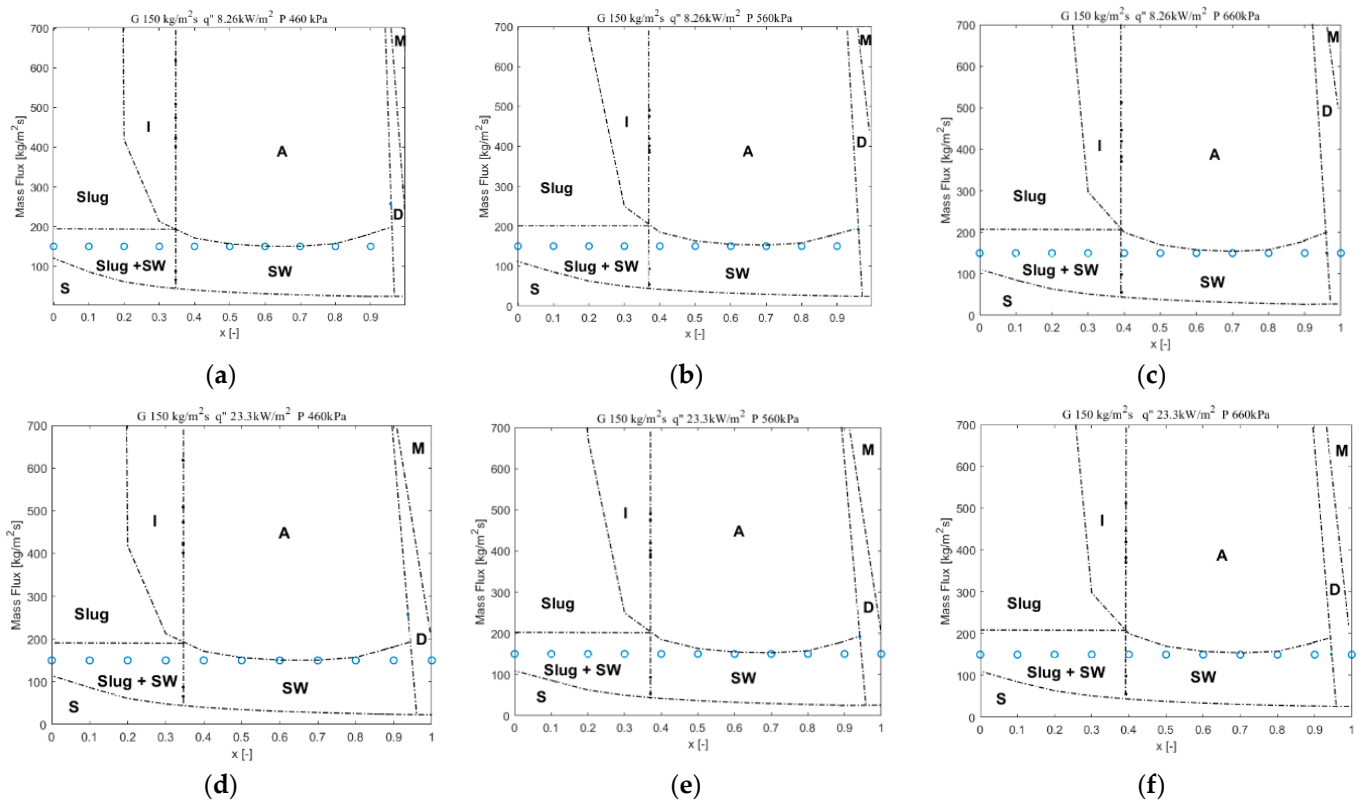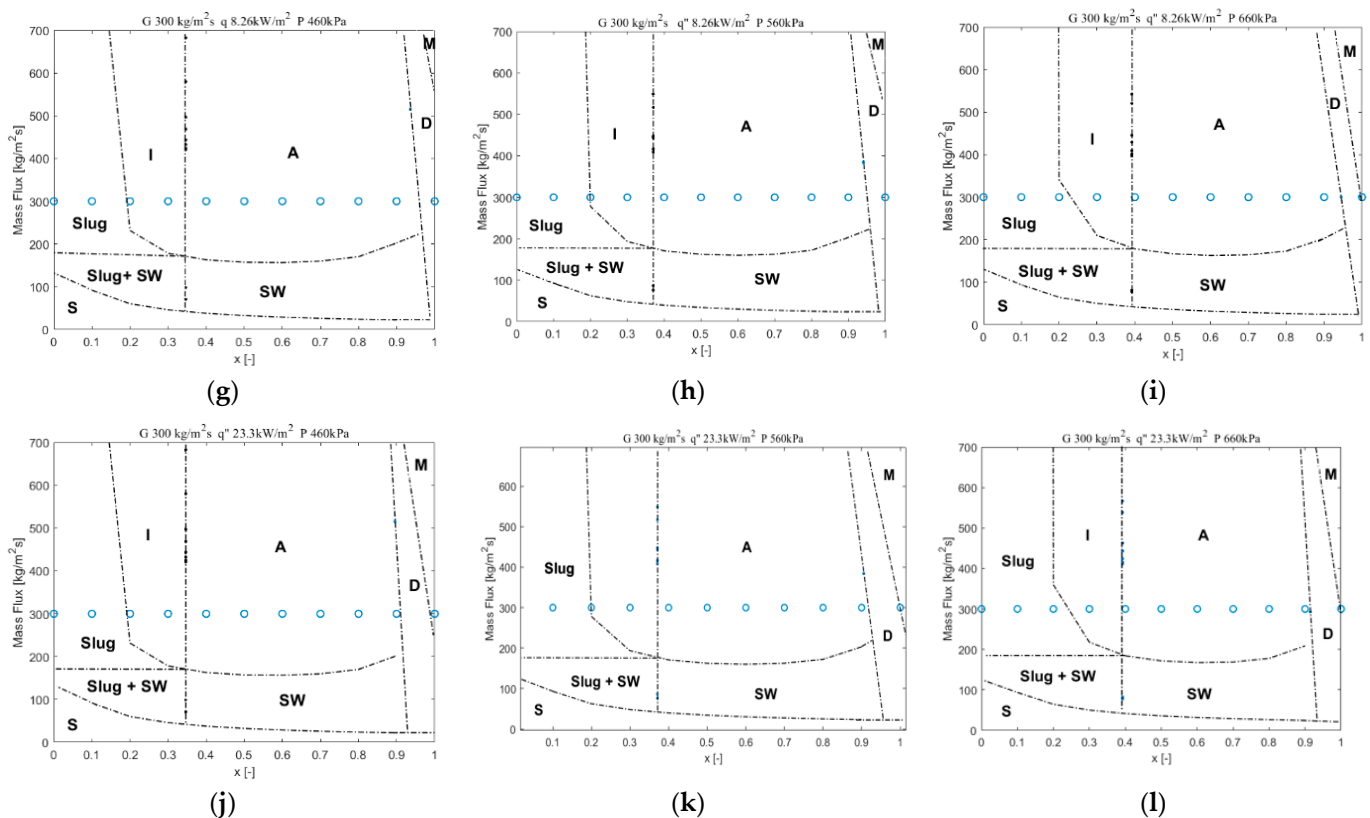

Figure 9. *Cont.*

Figure 9. Flow pattern predictions by Wojtan et al. for increasing saturation pressures from 460 kPa to 660 kPa at G 150 kg/m²s, q″ 8.26 kW/m² (**a–c**), G 150 kg/m²s, q″ 23.3 kW/m² (**d–f**), G 300 kg/m²s, q″ 8.26 kW/m² (**g–i**) and G 300 kg/m²s, q″ 23.3 kW/m² (**j–l**).

Figure 9a–f shows the flow patterns for an increasing saturation pressure at G 150 kg/(m²s), q″ 8.26 kW/m² (Figure 9a–c), and q″ 23.3 kW/m² (Figure 9d–f) as predicted by a well-known flow pattern map from Wojtan et al. The flow patterns predicted for these experimental conditions are a mixture of slug and stratified wavy, purely stratified wavy, and dryout. Increasing saturation pressure increases the vapor quality at which the flow patterns transition from mixed slug and stratified to purely stratified wavy. At saturation pressures of 460 kPa, 560 kPa, and 660 kPa, the transitions occur at vapor quality of 0.345, 0.370, and 0.395, respectively. These flow patterns are predicted because of insufficient refrigerant flow rate for the low mass flux of 150 kg/(m²s).

Figure 9g–l shows the flow patterns for an increasing saturation pressure of 460 kPa, 560 kPa, and 660 kPa at an increased mass flux of 300 kg/(m²s), heat flux of 8.26 kW/m² (Figure 9e–g), and 23.3 kw/m² (Figure 9h–l) as predicted by the flow pattern map from Wojtan et al. For these conditions, the flow patterns predicted are slug, intermittent, annular, dryout, and mist flow. Increasing saturation pressure increases the vapor quality at which the flow pattern transitions from intermittent flow to annular flow. In addition, at saturation pressures of 460 kPa, 560 kPa, and 660 kPa, the transitions occur at vapor qualities of 0.345, 0.370, and 0.395, respectively. These flow patterns are observed because of sufficient mass flux for increasing the flow rate during flow boiling.

3.3. Frictional Pressure Drop

The total pressure drop of a fluid is as a result of changes in kinetic energy, potential energy, and friction effect. For this reason, the pressure drop (ΔP) is the summation of the static pressure drop (ΔP_s) due to elevation head, momentum pressure drop (ΔP_m) due to

acceleration and frictional pressure drop $\left(\Delta P_f\right)$ due to the effect of frictional forces [29] given as:

$$\Delta P = \Delta P_s + \Delta P_m + \Delta P_f.$$

Because the tube for this experimental study is horizontal and the flow has minimal flashing with little heat losses, the static and momentum pressure drop were assumed to be negligible. The total pressure drop is thus the adiabatic frictional pressure drop that was recorded in the adiabatic test section for the same operating conditions the heat transfer coefficient was recorded using a differential pressure transducer.

Figure 10a–d shows the effect of saturation pressure on adiabatic frictional pressure drop. It can be observed that, for a constant mass flux and heat flux condition, the frictional pressure drop increases with vapor quality until a maximum is reached and then it deteriorates up to a vapor quality of 1 where it tends to linearize or increase slightly. With respect to saturation pressure, frictional pressure drop decreases with increasing saturation pressure. This is because, when saturation pressure increases, vapor density increases. This then decreases the vapor velocity and thus results in the observed trend of decreasing pressure drop with increasing saturation pressure.
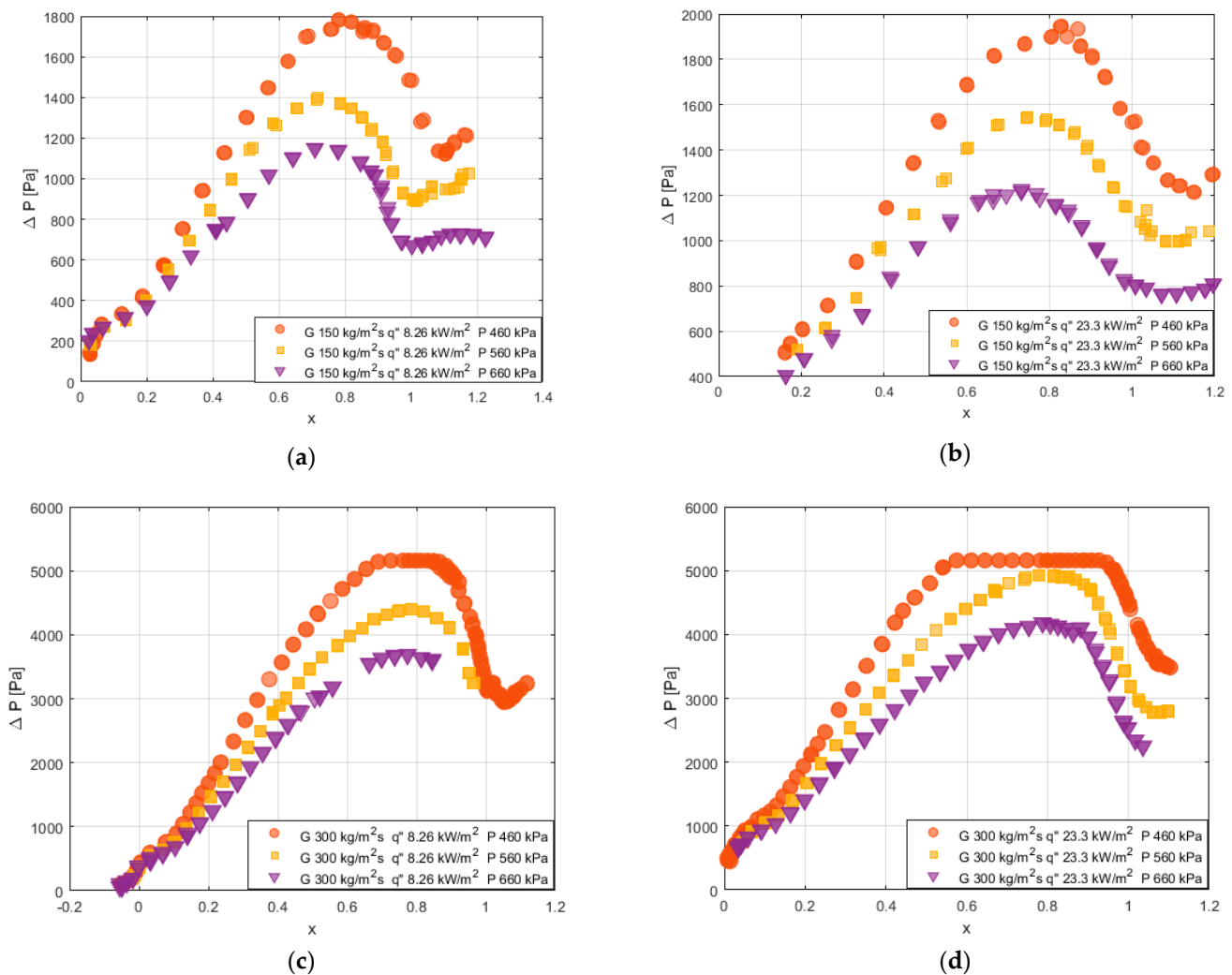

Figure 10. Effect of saturation pressure on adiabatic frictional pressure drop at (**a**) G 150 kg/m²s, q″ 8.26 kW/m², (**b**) G 150 kg/m²s, q″ 23.3 kW/m², (**c**) G 300 kg/m²s, q″ 8.26 kW/m² and (**d**) G 300 kg/m²s, q″ 23.3 kW/m².

3.4. Comparison of Experimental Results with Correlations of Heat Transfer Coefficient Developed Based on Different Theories

　　Statistical analysis of the study was performed by comparing experimental results obtained with different flow boiling heat transfer correlations and models developed based on different theories. Five different theoretical approaches upon which the selected models were formulated were considered for the statistical analysis. These are pool boiling type, superposition type, enhancement approach, asymptotic approach, and largest mechanism type. For pool boiling, we considered models by Cooper and Tran et al. [30,31], for the superposition model, we considered Bertsch et al. [32], for the enhancement type of model, Warrier et al.'s model [33] was considered, for asymptotic, Wattelet et al.'s model [34] and the model of Liu and Winterton [35] were considered. Kandlikar's model [36] was considered for largest mechanism type of model.

　　The results from the comparison of the experimental data with the predicted models are summarized in Tables 6–9 below where MRE is the mean relative error and MAE is the mean absolute error calculated by:

$$MRE = \frac{1}{N} \sum_{i=1}^{N} \left(\frac{h_{pred,i} - h_{exp,i}}{h_{exp,i}} \right)$$

$$MAE = \frac{1}{N} \sum_{i=1}^{N} \left(\frac{\left| h_{pred,i} - h_{exp,i} \right|}{h_{exp,i}} \right)$$

Table 6. Statistical analysis of the comparison between experimental heat transfer coefficient and prediction models at saturation pressure of 460 kPa.

Experimental Condition		P 460 kPa G 150 kg/m²s q″ 8.26 kW/m²	P 460 kPa G 150 kg/m²s q″ 23.3 kW/m²	P 460 kPa G 300 kg/m²s q″ 8.26 kW/m²	P 460 kPa G 300 kg/m²s q″ 23.3 kW/m²	All Data at 460 kPa
Cooper [30]	MRE %	−11.9	11.1	−27.7	3.5	−6.25
	MAE %	0.2	8.4	14.1	11.2	8.48
Tran et al. [31]	MRE %	−67.0	−61.4	8.0	43.7	−19.18
	MAE %	62.7	62.4	28.3	54.5	51.825
Bertsch et al. [32]	MRE %	−49.8	−65.8	−62.1	−70.0	−61.30
	MAE %	50.6	69.1	56.6	67.2	60.88
Warrier et al. [33]	MRE %	−88.7	−60.8	−103.5	−84.1	−84.28
	MAE %	94.7	59.0	99.4	95.6	87.18
Liu and Winterton [35]	MRE %	−19.2	−41.0	−15.4	−19.5	−23.78
	MAE %	0.39	30.9	28.1	7.6	16.75
Wattelet et al. [34]	MRE %	13.1	20.5	76.5	34.4	36.13
	MAE %	3.1	10.7	7.8	14.4	9.0
Kandlikar [36]	MRE %	38.6	52.8	−7.8	74.4	39.5
	MAE %	89.9	130.8	80.7	138.0	109.9

Table 7. Statistical analysis of the comparison between experimental heat transfer coefficient and prediction models at saturation pressure of 560 kPa.

Experimental Condition		P 560 kPa G 150 kg/m²s q″ 8.26 kW/m²	P 560 kPa G 150 kg/m²s q″ 23.3 kW/m²	P 560 kPa G 300 kg/m²s q″ 8.26 kW/m²	P 560 kPa G 300 kg/m²s q″ 23.3 kW/m²	All Data at 560 kPa
Cooper [30]	MRE %	5.2	64.7	−30.7	6.1	11.33
	MAE %	11.4	1.3	7.0	1.3	5.25
Tran et al. [31]	MRE %	−61.8	−44.4	0.6	43.3	−15.58
	MAE %	67.8	65.8	35.1	36.7	51.35
Bertsch et al. [32]	MRE %	−41.9	−55.0	−60.0	−68.5	−56.35
	MAE %	57.2	71.3	54.0	71.2	63.43
Warrier et al. [33]	MRE %	−87.4	−56.5	−103.9	−77.2	−81.25
	MAE %	94.9	56.8	99.2	86.9	84.45
Liu and Winterton [35]	MRE %	−22.0	−19.7	0.9	−27.2	−17.0
	MAE %	13.0	37.8	37.3	11.3	24.85
Wattelet et al. [34]	MRE %	6.6	65.1	−22.6	8.2	14.33
	MAE %	9.9	1.6	3.3	3.7	4.63
Kandlikar	MRE %	26.6	56.5	27.1	50.8	40.25
	MAE %	72.8	117.2	102.1	115.3	101.85

Table 8. Statistical analysis of the comparison between experimental heat transfer coefficient and prediction models at saturation pressure of 660 kPa.

Experimental Condition		P 660 kPa G 150 kg/m²s q″ 8.26 kW/m²	P 660 kPa G 150 kg/m²s q″ 23.3 kW/m²	P 660 kPa G 300 kg/m²s q″ 8.26 kW/m²	P 660 kPa G 300 kg/m²s q″ 23.3 kW/m²	All Data at 660 kPa
Cooper [30]	MRE %	2.8	110.4	−27.4	33.1	29.73
	MAE %	19.0	6.0	12.5	1.9	9.85
Tran et al. [31]	MRE %	−63.9	−31.4	1.9	73.7	−4.93
	MAE %	71.6	69.3	22.9	28.1	47.98
Bertsch et al. [32]	MRE %	−42.9	−41.5	−56.8	−64.4	−51.4
	MAE %	61.7	73.9	58.4	72.5	66.63
Warrier et al. [33]	MRE %	−87.0	−48.1	−104.1	−76.7	−78.98
	MAE %	95.5	61.4	101.9	88.7	86.88
Liu and Winterton [35]	MRE %	−26.8	−2.4	8.4	−16.9	−9.43
	MAE %	21.8	44.4	42.3	16.4	31.22
Wattelet et al. [34]	MRE %	4.2	110.9	−18.2	35.3	33.05
	MAE %	17.6	5.7	1.3	0.5	6.28
Kandlikar [36]	MRE %	24.1	80.6	42.0	48.9	48.90
	MAE %	61.9	101.7	86.2	115.1	91.23

Table 9. Statistical analysis of the comparison between experimental heat transfer coefficient and prediction models for all data at saturation pressures of 460–660 kPa.

Experimental Pressure	P 460 kPa		P 560 kPa		P 660 kPa	
	MRE %	MAE %	MRE %	MAE %	MRE %	MAE %
Cooper [30]	−6.25	8.48	11.33	5.25	29.73	9.85
Tran et al. [31]	−19.18	51.825	−15.58	51.35	−4.93	47.98
Bertsch et al. [32]	−61.30	60.88	−56.35	63.43	−51.4	66.63
Warrier et al. [33]	−84.28	87.18	−81.25	84.45	−78.98	86.88
Liu and Winterton [35]	−23.78	16.75	−17.0	24.85	−9.43	31.22
Wattelet et al. [34]	36.13	9.0	14.33	4.63	33.05	6.28
Kandlikar [36]	39.5	109.9	40.25	101.85	48.90	91.23

Here, h_{pred} and h_{exp} are the predicted and experimental heat transfer coefficient, respectively. N is the number of data points collected.

Figure 11a–l depicts the graphical representation of the comparison between each experimental result measured and the calculated heat transfer coefficient developed based on different theoretical assumptions at the different saturation conditions investigated in this study.

For saturation pressure of 460 kPa, the models that predicted the experimental data with an MAE of less than 30% were Cooper [30], followed by Wattalet et al. [34] and Liu and Winterton [35] with MAE of 8.48%, 9.0%, and 16.75%, respectively.

For saturation pressure of 560 kPa, the models of Wattelet et al. [34], Cooper [30] and Liu, and Winterton [30] best predicted the experimental data within a range of 30% with a low MAE of 4.63%, 5.25%, and 24.85%, respectively.

The models of Wattelet et al. [34] and Cooper [30] best predicted the experimental conditions at 660 kPa with a low MAE of 6.28% and 9.85%, respectively.

Overall, Cooper's model [30] and Wattelet et al.'s model [34] were the best predictors of the experimental data. Cooper's model [30] was developed based on pool boiling conditions where the effect of vapor quality was not considered and nucleate boiling dominated the heat transfer. This thus justifies why the dominant mechanism responsible for controlling heat transfer for most of the conditions was nucleate boiling. Wattelet et al.'s model [34] is also an asymptotic model that considers the summed effects of both nucleate boiling and convective boiling heat transfer. In most of these conditions, nucleate boiling dominated, and thus its ability to predict most of the data with low MAE.
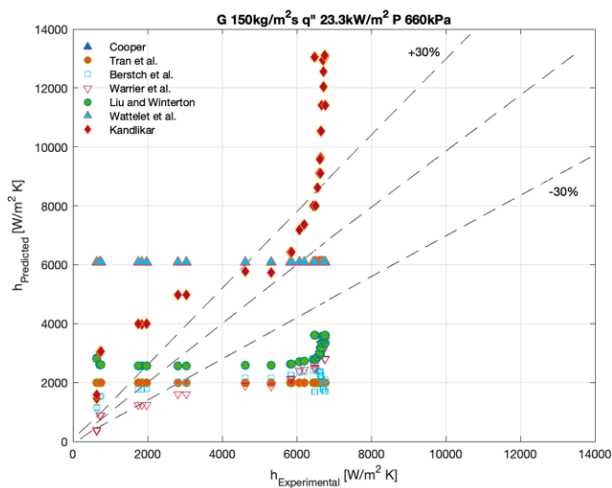
Figure 12a–l shows the trend of how each predictive model is able to capture the experimental trend compared with experimental data over the entire range of vapor qualities. Generally, none of the models selected are able to satisfactorily trace the heat transfer coefficient over the entire range of vapor quality.
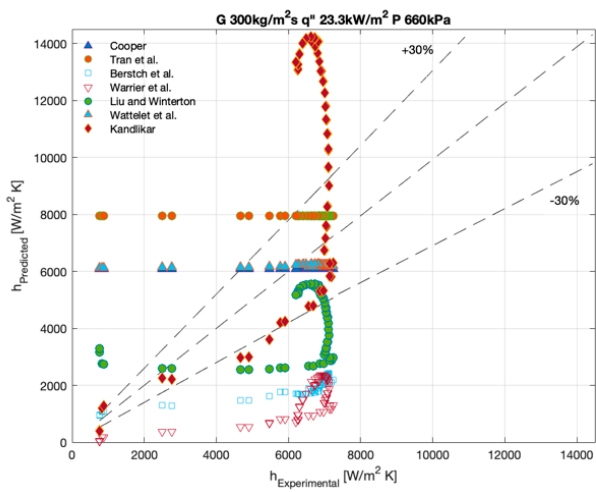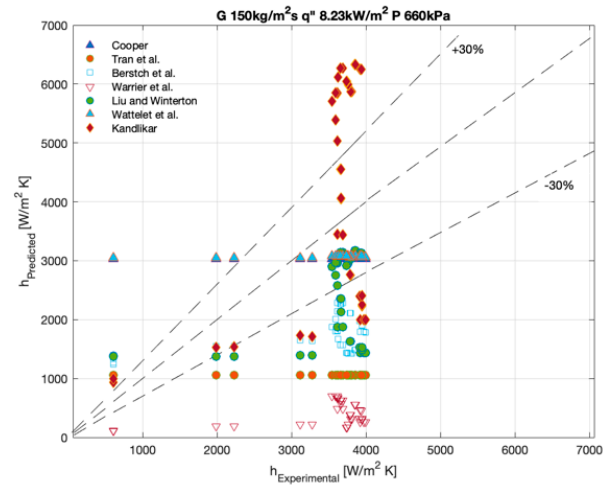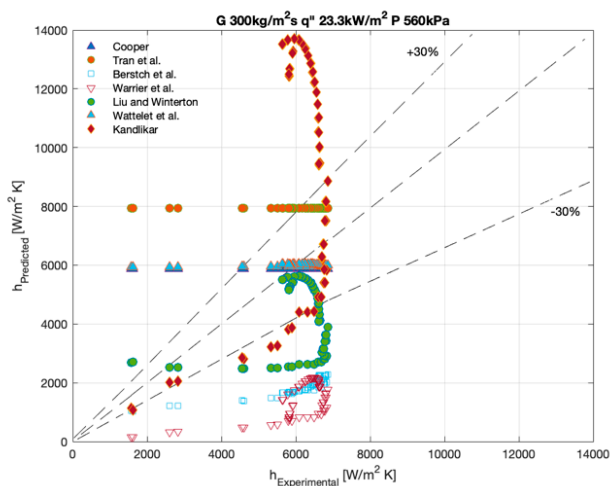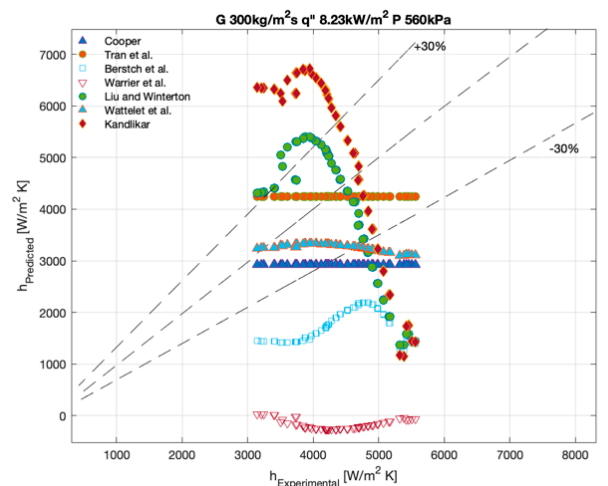
(**a**)
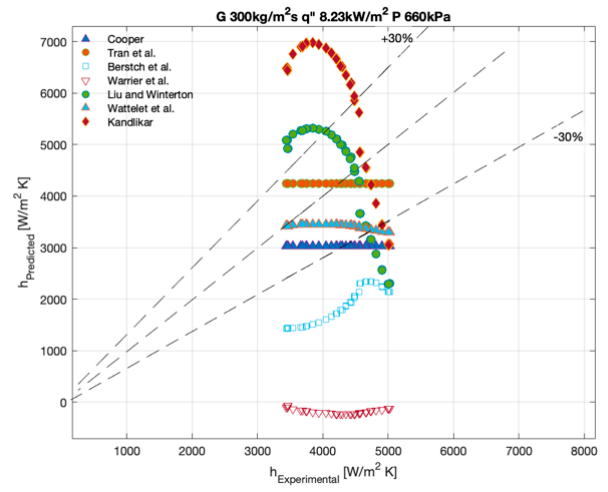
(**b**)

(**c**)

(**d**)

(**e**)

(**f**)

Figure 11. *Cont*.

(**g**)

(**h**)

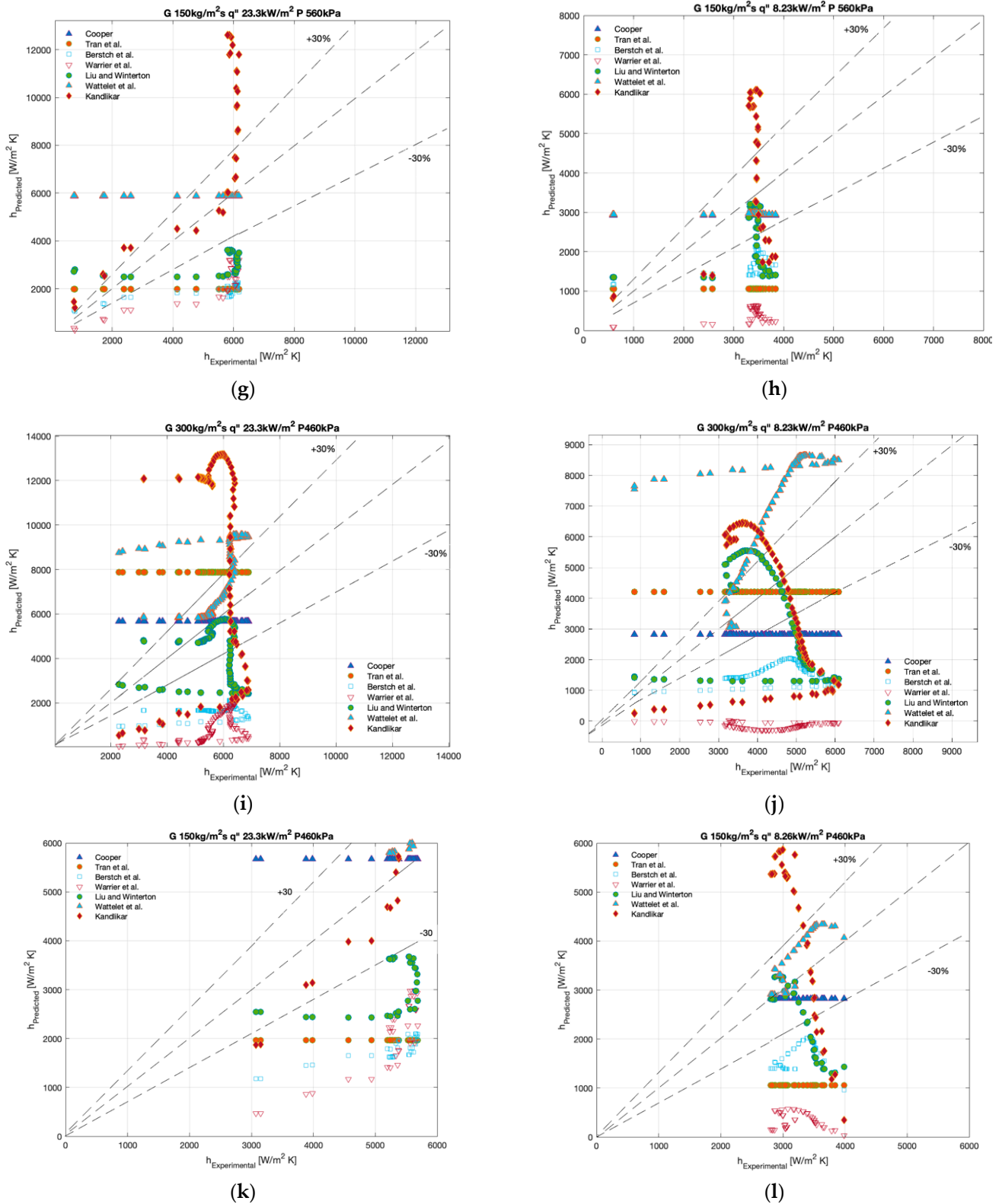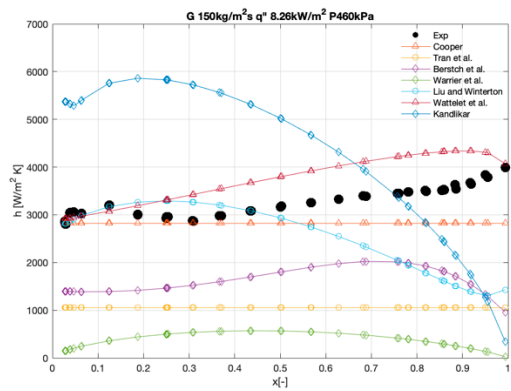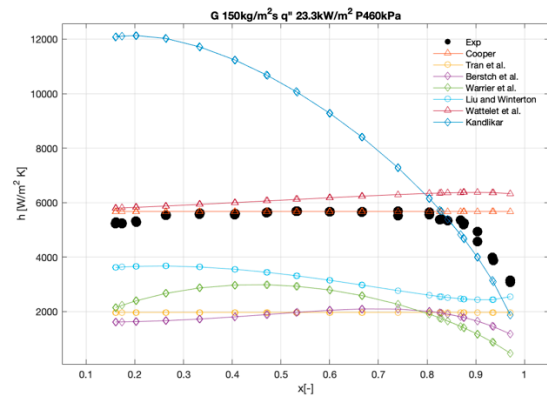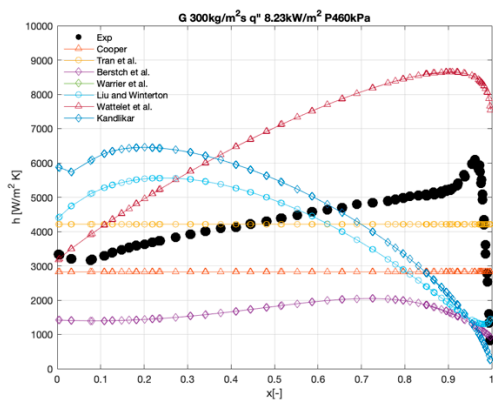(**i**)

(**j**)

(**k**)

(**l**)

Figure 11. (**a–l**) Comparison between each experimental result measured at conditions of G 150–300 kg/m²s, q″ 8.26–23.3 kW/m², P 460–660 kPa and the calculated heat transfer coefficient developed based on different theoretical assumptions by Cooper [30], Tran et al. [31], Berstch et al. [32], Warrier et al. [33], Wattelet et al. [34], Liu and Winterton [35] and Kandlikar [36].
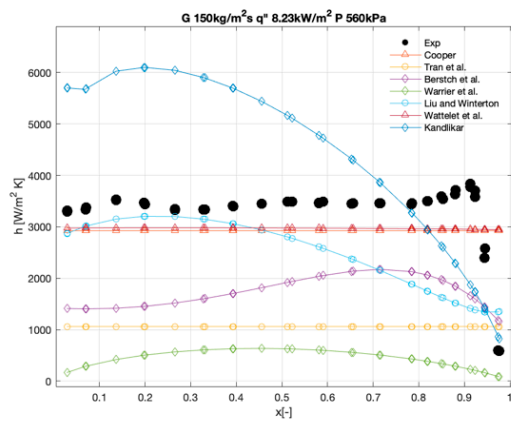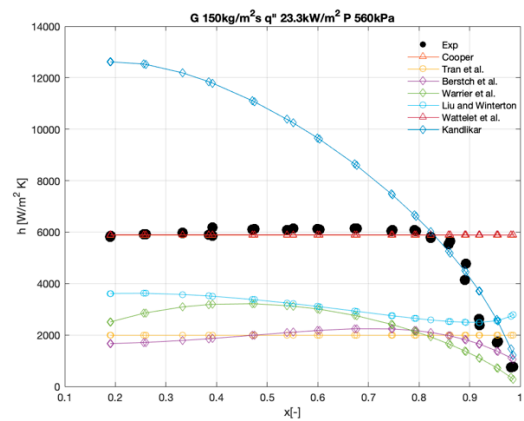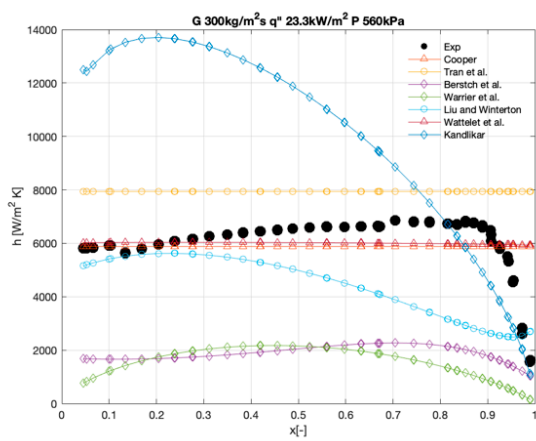
(**a**)

(**b**)

(**c**)
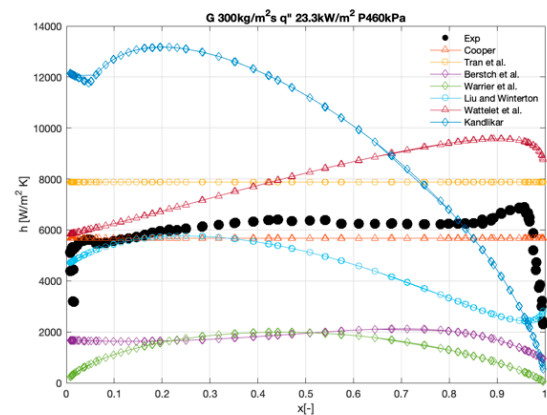
(**d**)

(**e**)

(**f**)

Figure 12. *Cont*.

(g)
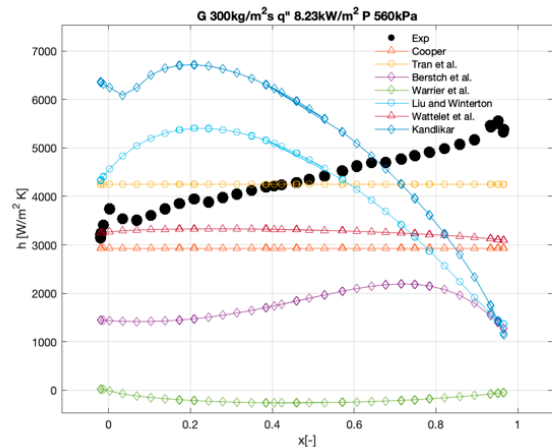
(h)
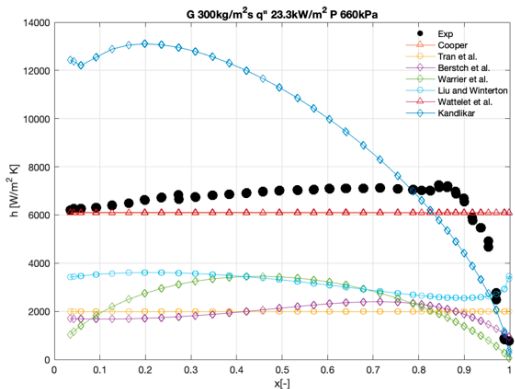
(i)

(j)

(k)

(l)

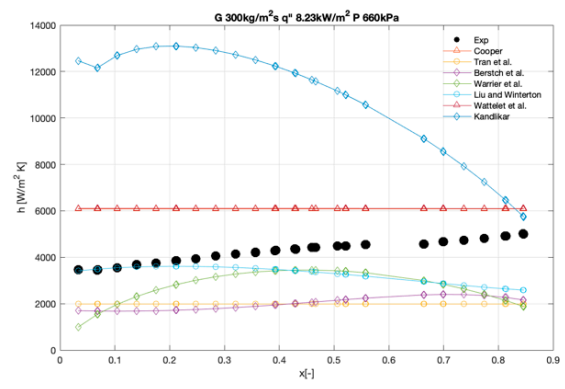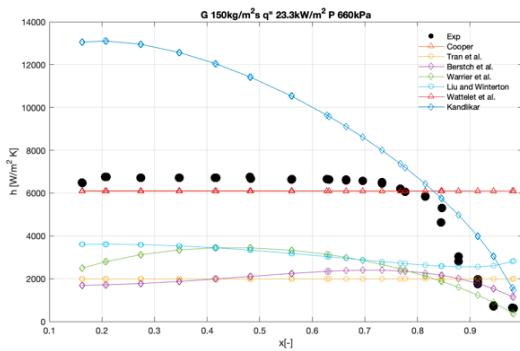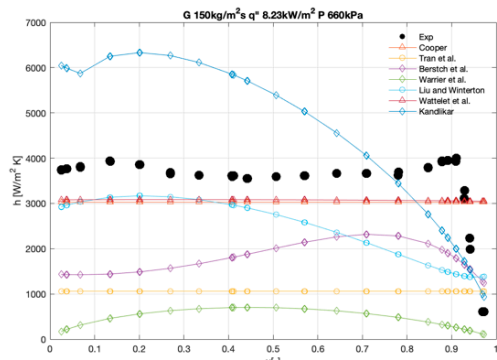**Figure 12.** (**a**–**l**) Comparison of how predictive models of Cooper [30], Tran et al. [31], Berstch et al. [32], Warrier et al. [33], Wattelet et al. [34], Liu and Winterton [35] and Kandlikar [36] are able to capture experimental trend over vapor quality for conditions of G 150–300 kg/m^{2}s, q″ 8.26–23.3 kW/m^2, P 460–660 kPa.

For cases where convective boiling dominated the heat transfer as discussed in Section 3 where the heat transfer coefficient increases with vapor quality, (such as in Figure 7), the models of Berstch et al. [32] and Wattelet et al. [34] are able to predict the trend of heat transfer coefficient over a wide range of vapor quality up to dryout.

For nucleate boiling-dominated heat transfer where the heat transfer coefficient did not respond significantly with vapor quality such as in Figures 5, 6 and 8, models of Cooper [30], Wattelet et al. [34], Tran et al. [31], and Berstch et al. [32] are able to capture the trend of heat transfer over a wide range of vapor quality up to dryout. Although these

models are able to capture the trend of the heat transfer coefficient with vapor quality until dryout is reached, they either over-predict or under-predict the experimental data except Cooper's model [30], which is able to both capture the trend of the heat transfer coefficient and accurately predict the experimental data for conditions of G 150 kg/(m^{2}s), q 23.3 kW/m^2, P$_{sat}$ 460 kPa, and 560 kPa before dryout incipience.

4. Conclusions

In this study, the extensive evaluation of the heat transfer coefficient, flow patterns, and pressure drop was conducted for three saturation pressures in a horizontal smooth tube of 5 mm internal diameter using R134a as the working fluid. The study investigated the effect of saturation pressure for mass fluxes of 150–300 kg/m^{2}s and heat fluxes of 8.26–23.3 kW/m^2 which are typical of refrigeration and air conditioning applications. The flow patterns observed during the study were predicted with a well-known flow pattern map. The experimental results were compared with seven (7) correlations developed based on different theories to find which correlation best predicts the experimental data. These included the pool boiling type, superposition type, enhancement approach, asymptotic approach, and largest mechanism type. The following conclusions were made:

- At low mass flux, increasing saturation pressure increased the heat transfer coefficient. This effect was more pronounced in the low vapor quality region and the dominant mechanism was nucleate boiling.
- At high mass flux, increasing saturation pressure led to an insignificant increase in the heat transfer coefficient. At high mass flux but low heat flux, the heat transfer coefficient increased with vapor quality, indicating convective boiling dominance. However, for high heat flux, the heat transfer coefficient was linear over vapor quality, indicating nucleate boiling dominance.
- Pressure drop was observed to decrease with increasing saturation pressure.
- Increasing saturation pressure increased the vapor quality at which the flow pattern transitions from intermittent flow to annular flow. The flow patterns predicted by Wojtan's flow pattern map were a mixture of slug and stratified wavy and purely stratified wavy for low mass fluxes. For increased mass fluxes, the flow patterns predicted were slug, intermittent, annular, and dry out.
- Cooper's model was the best predictor of the experimental data and the trend of heat transfer followed by the models of Wattalete et al. and Liu and Winterton.

Author Contributions: Conceptualization, E.G.B.; methodology, E.G.B.; formal analysis, E.G.B. and T.V.; investigation, E.G.B., T.V. and P.D.; writing—original draft preparation, E.G.B.; writing—review and editing, E.G.B., T.V. and P.D.; supervision, T.V.; project administration, E.G.B. All authors have read and agreed to the published version of the manuscript.

Data Availability Statement: All data are available from the authors on request.

Nomenclature

A	Cross section area (m^2)
c_p	Specific heat capacity
D	Channel diameter (m)
h	Heat transfer coefficient (W/(m^2 K))
G	Mass flux (kg/(m^{2}s))
g	Acceleration due to gravity (ms^{-2})
k	Thermal conductivity of liquid (W/(m K))
Nu	Nusselt number (hD/k)

Pr	Prandtl number
PrL	Liquid phase Prandtl number
PrV	Vapor phase Prandtl number
P	Total heat len (W)
q''	Heat flux (Wm^{-2})
ReL	Liquid Reynolds number
$Tsub$	Inlet subcooling (K)
ReV	Vapor Reynolds number
$Re2\phi$	Two-phase Reynolds
x	Vapor quality
hlv	Latent heat of vaporization (J/(kg K)
hl	Specific enthalpy of liquid (J/(kg K))
Tw,i	Inner wall temperature (K)
Tf	Fluid temperature (K)

References

1. Copetti, J.B.; Macagnan, M.H.; Zinani, F.; Kunsler, N.L. Flow boiling heat transfer and pressure drop of R-134a in a mini tube: An experimental investigation. *Exp. Therm. Fluid Sci.* **2011**, *35*, 636–644. [CrossRef]
2. Mortada, S.; Zoughaib, A.; Arzano-Daurelle, C.; Clodic, D. Boiling heat transfer and pressure drop of R-134a and R-1234yf in minichannels for low mass fluxes. *Int. J. Refrig.* **2012**, *35*, 962–973. [CrossRef]
3. Oudah, M.H.; Mejbel, M.K.; Allawi, M.K. R134a flow boiling heat transfer (FBHT) characteristics in a refrigeration system. *J. Mech. Eng. Res. Dev.* **2021**, *44*, 69–83.
4. Kim, S.-M.; Mudawar, I. Review of databases and predictive methods for heat transfer in condensing and boiling mini/micro-channel flows. *Int. J. Heat Mass Transf.* **2014**, *77*, 627–652. [CrossRef]
5. Charnay, R. Experimental Study of Flow Boiling in Horizontal Minichannels at High Saturation Temperature. Doctoral Dissertation, INSA de Lyon, Villeurbanne, France, 2015.
6. Kandlikar, S.G. Heat Transfer Mechanisms During Flow Boiling in Microchannels. *J. Heat Transf.* **2004**, *126*, 8–16. [CrossRef]
7. Charnay, R.; Revellin, R.; Bonjour, J. Flow boiling characteristics of R-245fa in a minichannel at medium saturation temperatures. *Exp. Therm. Fluid Sci.* **2014**, *59*, 184–194. [CrossRef]
8. Paul, S.; Fernandino, M.; Dorao, C.A. On the scaling of convective boiling heat transfer coefficient. *Int. J. Heat Mass Transf.* **2021**, *164*, 120589. [CrossRef]
9. Dorao, C.A.; Fernandez, O.B.; Fernandino, M. Experimental Study of Horizontal Flow Boiling Heat Transfer of R134a at a Saturation Temperature of 18.6 °C. *J. Heat Transf.* **2017**, *139*, 111510. [CrossRef]
10. Charnay, R.; Revellin, R.; Bonjour, J. Flow boiling heat transfer in minichannels at high saturation temperatures: Part I—Experimental investigation and analysis of the heat transfer mechanisms. *Int. J. Heat Mass Transf.* **2015**, *87*, 636–652. [CrossRef]
11. Wang, L.; Chen, M.; Groll, M. Flow Boiling Heat Transfer Characteristics of R134a in a Horizontal Mini Tube. *J. Chem. Eng. Data* **2009**, *54*, 2638–2645. [CrossRef]
12. Ali, R. Dryout Incipience and Critical Heat Flux in Saturated Flow Boiling of Refrigerants in a Vertical Uniformly Heated Microchannel. In Proceedings of the ASME 2008 6th International Conference on Nanochannels, Microchannels, and Minichannels, Darmstadt, Germany, 23–25 June 2008; pp. 1–8.
13. van den Bergh, W.J.; Moran, H.R.; Dirker, J.; Markides, C.N.; Meyer, J.P. Effect of low heat and mass fluxes on the boiling heat transfer coefficient of R-245fa. *Int. J. Heat Mass Transf.* **2021**, *180*, 121743. [CrossRef]
14. Hellenschmidt, D.; Petagna, P. Effects of saturation temperature on the boiling properties of carbon dioxide in small diameter pipes at low vapour quality: Heat transfer coefficient. *Int. J. Heat Mass Transf.* **2021**, *172*, 121094. [CrossRef]
15. Greco, A.; Vanoli, G.P. Flow-boiling of R22, R134a, R507, R404A and R410A inside a smooth horizontal tube. *Int. J. Refrig.* **2005**, *28*, 872–880. [CrossRef]
16. Celen, A.; Dalkılıç, A.S. A complete evaluation method for the experimental data of flow boiling in smooth tubes. *Int. Commun. Heat Mass Transf.* **2017**, *89*, 108–121. [CrossRef]
17. Eckels, S.; Pate, M. An experimental comparison of evaporation and condensation heat transfer coefficients for HFC-134a and CFC-12. *Int. J. Refrig.* **1991**, *14*, 70–77. [CrossRef]
18. Xu, Y.; Fang, X.; Li, G.; Li, D.; Yuan, Y. An experimental study of flow boiling heat transfer of R134a and evaluation of existing correlations. *Int. J. Heat Mass Transf.* **2016**, *92*, 1143–1157. [CrossRef]
19. Guo, Q.; Li, M.; Tian, X. Experimental study on flow boiling heat transfer characteristics of R134a, R245fa and R134a/R245fa mixture at high saturation temperatures. *Int. J. Therm. Sci.* **2019**, *150*, 106195. [CrossRef]
20. Grauso, S.; Mastrullo, R.; Mauro, A.; Thome, J.; Vanoli, G.P. Flow pattern map, heat transfer and pressure drops during evaporation of R-1234ze(E) and R134a in a horizontal, circular smooth tube: Experiments and assessment of predictive methods. *Int. J. Refrig.* **2013**, *36*, 478–491. [CrossRef]
21. Saitoh, S.; Daiguji, H.; Hihara, E. Effect of tube diameter on boiling heat transfer of R-134a in horizontal small-diameter tubes. *Int. J. Heat Mass Transf.* **2005**, *48*, 4973–4984. [CrossRef]

22. Balachander, P.; Raja, B. Investigation on the boiling heat transfer characteristics of R404A and R134a under stratified flow condition. *Heat Mass Transf.* **2015**, *51*, 825–835. [CrossRef]
23. Dorao, C.A.; Drewes, S.; Fernandino, M. Can the heat transfer coefficients for single-phase flow and for convective flow boiling be equivalent? *Appl. Phys. Lett.* **2018**, *112*, 064101. [CrossRef]
24. Mahmoud, M.M.; Karayiannis, T.G. Heat transfer correlation for flow boiling in small to micro tubes. *Int. J. Heat Mass Transf.* **2013**, *66*, 553–574. [CrossRef]
25. Charnay, R.; Revellin, R.; Bonjour, J. Flow boiling heat transfer in minichannels at high saturation temperatures: Part II—Assessment of predictive methods and impact of flow regimes. *Int. J. Heat Mass Transf.* **2015**, *87*, 653–672. [CrossRef]
26. Fang, X. A new correlation of flow boiling heat transfer coefficients based on R134a data. *Int. J. Heat Mass Transf.* **2013**, *66*, 279–283. [CrossRef]
27. Bediako, E.G.; Dančová, P.; Vít, T. Experimental Study of Horizontal Flow Boiling Heat Transfer Coefficient and Pressure Drop of R134a from Subcooled Liquid Region to Superheated Vapor Region. *Energies* **2022**, *15*, 681. [CrossRef]
28. Lemmon, E.; McLinden, M.; Huber, M. NIST Standard Reference Database 23-NIST Thermodynamic and Transport Properties Refprop, Version 7.0. 2002. Available online: https://www.nist.gov/publications/nist-standard-reference-database-23-nist-thermodynamic-and-transport-properties-refprop (accessed on 26 October 2021).
29. Wojtan, L.; Ursenbacher, T.; Thome, J.R. Investigation of flow boiling in horizontal tubes: Part I—A new diabatic two-phase flow pattern map. *Int. J. Heat Mass Transf.* **2005**, *48*, 2955–2969. [CrossRef]
30. Cooper, M.G. Heat Flow Rates in Saturated Nucleate Pool Boiling-A Wide-Ranging Examination Using Reduced Properties. *Adv. Heat Transf.* **1984**, *16*, 157–239. [CrossRef]
31. Tran, T.N.; Wambsganss, M.W.; France, D.M. Small circular- and rectangular-channel boiling with two refrigerants. *Int. J. Multiph. Flow* **1996**, *22*, 485–498. [CrossRef]
32. Bertsch, S.S.; Groll, E.A.; Garimella, S.v. Refrigerant flow boiling heat transfer in parallel microchannels as a function of local vapor quality. *Int. J. Heat Mass Transf.* **2008**, *51*, 4775–4787. [CrossRef]
33. Warrier, G.R.; Dhir, V.K.; Momoda, L.A. Heat transfer and pressure drop in narrow rectangular channels. *Exp. Therm. Fluid Sci.* **2002**, *26*, 53–64. [CrossRef]
34. Wattelet, J.P.; Chato, J.C.; Souza, A.L.; Christoffersen, B.R. Evaporative Characteristics of R-134a, MP-39, and R-12 at Low Mass Fluxes. 1993. Available online: http://www.ideals.illinois.edu/handle/2142/9736 (accessed on 7 October 2022).
35. Liu, Z.; Winterton, R.H.S. A general correlation for saturated and subcooled flow boiling in tubes and annuli, based on a nucleate pool boiling equation. *Int. J. Heat Mass Transf.* **1991**, *34*, 2759–2766. [CrossRef]
36. Kandlikar, S.G. A General Correlation for Saturated Two-Phase Flow Boiling Heat Transfer Inside Horizontal and Vertical Tubes. *J. Heat Transf.* **1990**, *112*, 219–228. [CrossRef]